Low-*k* Interlayer Dielectric Materials: Synthesis and Properties of Alkoxy-Functional Silsesquioxanes

Kai Su,* Duane R. Bujalski, Katsuya Eguchi, Glenn V. Gordon, Duan-Li Ou, Pierre Chevalier, Sanlin Hu, and Ronald P. Boisvert

Dow Corning Corporation, Midland, Michigan 48686-0995

Received June 24, 2004. Revised Manuscript Received January 6, 2005

Two new types of silsesquioxanes, $(HSiO_{3/2})_x[(^tBuO)SiO_{3/2}]_z$ or T^HQ and $(HSiO_{3/2})_x(RSiO_{3/2})_y[(^tBuO)SiO_{3/2}]_z$ or T^HT^RQ (R = octadecyl), were synthesized and studied as low-*k* dielectric materials for electronic applications. The materials were prepared by cohydrolysis and condensation of alkoxy monomers, $(AcO)_2Si(O^tBu)_2$, $HSi(OEt)_3$, and $CH_3(CH_2)_{17}Si(OMe)_3$. Spectroscopic data supported retention of tertiary alkoxy groups [$(^tBuO)SiO_{3/2}$ or $(^tBuO)_2SiO_{2/2}$] and presence of silanol. The molecular weight of $(HSiO_{3/2})_x[(^tBuO)SiO_{3/2}]_z$ increased with the T/Q ratio, while that for $(HSiO_{3/2})_x(RSiO_{3/2})_y[(^tBuO)SiO_{3/2}]_z$ exhibited less dependence on composition. The *tert* butoxy groups were eliminated in both materials at low temperatures (<450 °C), and subsequent decomposition of octadecyl group (R) in $(HSiO_{3/2})_x(RSiO_{3/2})_y[(^tBuO)SiO_{3/2}]_z$ occurred through cleavage and re-distribution of carbon−carbon bonds (430−550 °C). Heating at 450 °C for 2 h afforded porous solids. The total pore volume of materials derived from $(HSiO_{3/2})_x[(^tBuO)SiO_{3/2}]_z$ determined by nitrogen sorption porosimetry increased with increasing Q content up to 0.313 cm^3/g or 38% porosity by volume. The porosity for $(HSiO_{3/2})_x(RSiO_{3/2})_y[(^tBuO)SiO_{3/2}]_z$ ranged from 32 to 54% (0.349−0.701 cm^3/g), which represented an ∼10% increase over $(HSiO_{3/2})_x[(^tBuO)SiO_{3/2}]_z$. Thin films prepared from $(HSiO_{3/2})_x[(^tBuO)SiO_{3/2}]_z$ exhibited a modulus between 10 and 19 GPa, but had a high dielectric constant due to residual silanol. Incorporation of $RSiO_{3/2}$ group allowed for formation of porous materials with low silanol contents. The dielectric constant and modulus of $(HSiO_{3/2})_x(RSiO_{3/2})_y[(^tBuO)SiO_{3/2}]_z$ were in the range of 1.7−2.6 and 1.8−4.7 GPa, respectively.

Introduction

Continuous improvements of integrated circuit (IC) devices to smaller feature sizes and faster speeds have reached a point where the interconnect signal delay, or resistance−capacitance (*RC*) delay, becomes comparable to transistor gate delay. More technologically advanced ICs with smaller feature sizes will require interlayer dielectric materials with lower dielectric constants (*k*) than current silicon dioxide to prevent electronic cross-talk and also to lower power consumption.[1,2] As a result, a flurry of activities have occurred in the past years to develop low-*k* options including porous materials, as well as organic spin-on polymers.[3−6]

Silsesquioxanes, which can be viewed as a hybrid of silica and organics, have lower *k* values than SiO_2, good thermal stability, and attractive mechanical properties. Hydrogen silsesquioxane (HSQ), developed at Dow Corning Corporation has a *k* of 2.8.[7−9] The porous version of HSQ, prepared by blending HSQ with a high boiling organic solvent followed by rapid cure and high-temperature elimination of volatiles, can provide *k* values from 1.5 to 2.5.[10,11] A number of research groups also reported methyl silsesquioxane (MSQ)[12,13] or porous MSQ-based low-*k* materials.[14−22] The

* Corresponding author. E-mail: k.su@dowcorning.com.

(1) Bohr, M. T. In *Proceedings of the 1995 IEEE International Electronic Device Meeting, Washington, DC, Dec. 10−13*; IEEE: Piscataway, NJ, 1995; pp 241−442.
(2) Bohr, M. T. In *Advanced Metallization and Interconnect Systems for ULSI Applications*; Havemann, R., Schmitz, J., Komiyama, H., Tsubouchi, K., Eds.; Materials Research Society: Pittsburgh, PA, 1996; pp 3−10.
(3) Hendricks, N. H. *Mater. Res. Soc. Symp. Proc.* **1997**, *443*, 3−14.
(4) Maex, K.; Baklanov, M. R.; Dhamiryan, D.; Lacopi, F.; Brongersma, S. H.; Yanovitskaya, Z. S. *J. Appl. Phys.* **2003**, *93*, 8793−8841.
(5) Hawker, C. J.; Hedrick, J. L.; Miller, R. D.; Volksen, W. *Mater. Res. Bull.* **2000**, *25*, 54−58.
(6) Martin, S. J.; Godschalx, J. P.; Mills, M. E.; Shaffer, E. O., II; Townsend, P. H. *Adv. Mater.* **2000**, *12*, 1769−1778.
(7) Collins, W.; Frye, C. U.S. Patent 3,615,272, 1968.
(8) Frye, C. L.; Collins, W. T. *J. Am. Chem. Soc.* **1970**, *92*, 5586.
(9) Haluska, L. A.; Michael, K. W.; Tarhay, L. U.S. Patent 4,753,856, 1988.
(10) Chung, K.; Moyer, E. S.; Spaulding, M. U.S. Patent 6,231,989, 2001.
(11) Zhong, B.; Spaulding, M.; Albaugh, J.; Moyer, E. S. *Polym. Mater.: Sci. Eng.* **2002**, *87*, 440−441.
(12) Chua, C. T.; Sarkar, G.; Chooi, S. Y. M.; Chan, L. *J. Mater. Sci. Lett.* **1999**, *18*, 1437−1439.
(13) Ryan, E. T.; McKerrow, A. J.; Leu, J.; Ho, P. S. *Mater. Res. Soc. Bull.* **1997**, October, 49−54.
(14) Hendricks, N. H. *Mater. Res. Soc. Symp. Proc.* **1997**, *443*, 3−14.
(15) Nguyen, C.; Hawker, C. J.; Miller, R. D.; Huang, E.; Hedrick, J. L.; Gauderon, R.; Hilborn, J. G. *Macromolecules* **2000**, *33*, 4281−4284.
(16) Hedrick, J. L.; Miller, R. D.; Hawker, C. J.; Carter, K. R.; Volksen, W.; Yoon, D. Y.; Trollsas, M. *Adv. Mater.* **1998**, *10*, 1049−1053.
(17) Hawker, C. J.; Hedrick, J. L.; Miller, R. D.; Volksen, W. *Mater. Res. Soc. Bull.* **2000**, *25*, 54−58.
(18) Hedrick, J. L.; Hawker, C. J.; Trollsas, M.; Remenar, J.; Yoon, D. Y.; Miller, R. D. *Mater. Res. Soc. Symp. Proc.* **1998**, *519*, 65−75.
(19) Nguyen, C. V.; Carter, K. R.; Hawker, C. J.; Hedrick, J. L.; Jaffe, R. L.; Miller, R. D.; Remenar, J. F.; Rhee, H. W.; Rice, P. M.; Toney, M. F.; Trollsas, M.; Yoon, D. Y. *Chem. Mater.* **1999**, *11*, 3080−3085.
(20) Kohl, A. T.; Mimna, R.; Shick, R.; Rhodes, L.; Wang, Z. L.; Kohl, P. A. *Electrochem. Solid State Lett.* **1999**, *2*, 77−79.
(21) Yang, S.; Mirau, P. A.; Pai, C.-S.; Nalamasu, O.; Reichmanis, E.; Lin,; E. K.; Lee, H.-J.; Gidley, D. W.; Sun, J. *Chem. Mater.* **2001**, *13*, 2762−1764.
(22) Yang, S.; Mirau, P. A.; Pai, C.-S.; Nalamasu, O.; Reichmanis, E.; Pai, J. C.; Obeng, Y. S.; Seputro, J.; Lin, E. K.; Lee, H.-J.; Sun, J.; Gidley, D. W. *Chem. Mater.* **2002**, *14*, 369−374.

10.1021/cm048993d CCC: $30.25
Published on Web 04/15/2005

use of chemically modified silsesquioxanes or copolymers that contained an organic spacer or pendent group which can be thermally degraded after cure to generate porosity was examined as an alternative option. The advantages of using homogeneous precursors include better control over composition and decomposition chemistry, which yield materials with small and narrow pore size distributions. Mikoshiba et al.[23] described siloxane-based resins with organic substituents that were oxidized at temperatures between 450 and 500 °C, which resulted in Angström-sized pores. Various silsesquioxane and silsesquioxane-silicate materials with *n*-alkyl substituents as the porogen were also disclosed in patent applications.[24,25] Researchers at Dow Corning also reported the use of functionalized silsesquioxanes to produce low-*k* coatings.[11,26−27]

This paper describes the synthesis of silsesquioxanes containing bulky Q-substituted tertiary alkoxy groups and the thermal cure thereof to provide coatings with low dielectric constants. Incorporation of a Q-substituted *tert*-alkoxy group into a silsesquioxane framework could generate a silica-modified resin in situ upon heat treatment, which could produce materials with improved mechanical properties. The use of *tert*-butoxy silanes as either molecular[28−35] or polymeric precursors[36−38] to prepare silicate ceramics has been studied, where some advantages include low-temperature decomposition and minimal residual carbon after ceramic conversion. The method described in this paper is useful for incorporating "silica" into various silsesquioxanes and the syntheses and properties of a broader breadth of materials will appear in subsequent publications.

Experimental Section

Materials. All organosiloxanes were obtained from Dow Corning Corporation as intermediates or purchased from Gelest, Inc.

Analytical Techniques. *Nuclei Magnetic Resonance.* Solution NMR spectra were collected from a Varian VXR400S spectrometer using either a 5-mm switchable probe or a 16-mm Si-free probe. All ^{1}H and ^{13}C chemical shifts were referenced to $(CH_3)_4Si$ (0.0 ppm). To ensure quantitative acquisition, the proper amount of $Cr(acac)_3$ was added to the test samples when collecting ^{29}Si NMR data. Solid-state (^{29}Si and ^{13}C) NMR spectra were acquired using a Varian Inova 400 equipped with a Varian 7-mm CP/MAS (cross-polarization/magic angle spinning) probe. Each test sample was loaded into a 7-mm Zirconia rotor and spun at 4 kHz. All solid-state NMR spectra were referenced to $(CH_3)_4Si$ and used hexamethyl benzene and tetrakis(trimethylsilyl)silane as secondary references for ^{13}C and ^{29}Si, respectively.

Fourier Transform Infrared Spectroscopy (FTIR) and Diffuse Reflectance Infrared Fourier Transform Spectroscopy (DRIFT). FTIR and DRIFT spectra were collected on a Perkin-Elmer 1600 Fourier transform infrared spectrometer. Appropriate diffuse reflectance attachment was used in acquiring the DRIFT spectra.

Size Exclusion Chromatography. SEC data were collected using a Waters 2690 Alliance System with two Polymer Laboratories PLgel Mixed-D (300 × 7.5 mm, 5 mm, 200−200 000 Da exclusion limit) styrene−divinyl benzene columns preceded by a PLgel guard column (50 × 7.5 mm, 5 mm). The detection system consisted of a Viscotek T60 multiple detector (viscosity and right-angle laser light scattering) and a Viscotek model 125 differential laser refractometer. HPLC-grade tetrahydrofuran (Fisher Scientific) was the eluent. The flow rate was 1 mL min^{-1} and a 100-mL injection volume was used, where the test samples were typically at a 1 wt/v% concentration.

Porosity Measurements. Nitrogen sorption porosimetry was conducted using a Quanta Chrome Autosorb 1MP system. The calculation procedure was performed by the Autosorb-1 software using the data taken from both the adsorption and desorption isotherms. The surface area was determined by the Brunauer−Emmett−Teller method.[39] The total pore volume was derived from the amount of vapor adsorbed at a relative pressure close to unity ($P/P_0 = 0.995$), by assuming that the pores were then filled with liquid adsorbate. The pore size distributions in the mesopore region were calculated using the Barrett−Joyner−Halenda method.[40]

Thermogravimetric Analysis and Evolved Gas Analysis. TGA was performed using a Thermoplus2 Rigaku TG-DTA 8101D model under a nitrogen flow from ambient to 800 °C with a ramp of 20 °C/min. Evolved gas analysis (EGA) was conducted using a Rigaku TG-MS interface. Gas chromatographic analyses were obtained on a Shimadzu GC-14A gas chromatograph employing a capillary column (DB5, 30 m × 0.25 mm). Helium was used as a carrier gas at 1 kg/cm^2 pressure. The mass spectra were recorded with a Shimadzu QP 5050A quadrupole mass spectrometer. The peak identification was carried out by electron ionization (70 eV), scanning from 16 to 900 amu with 1 s frequency.

Thin Film Thickness and Dielectric Constant Measurements. Thickness measurements of the films were performed using a J. A. Woollam M-88 spectroscopic ellipsometer equipped with WVASE32 software for data analysis. Dielectric measurements were determined from capacitance measurements on metal−insulator−semiconductor (MIS) capacitors using a HP4194A impedance/gain-phase analyzer. Capacitance measurements were taken over a frequency range of 10^2 to 10^7 Hz on electrodes of three different diameters (3.20, 4.85, and 6.40 mm). The reported dielectric constants were derived from measurements performed at 1 MHz.

Modulus and Hardness Measurements. Modulus and hardness were measured using a Hysitron Triboscope nanomechanical testing instrument equipped with a Berkovich diamond indenter. Hardness and reduced modulus values were determined at a penetration depth

(23) Mikoshiba, S.; Hayase, S. *J. Mater. Chem.* **1999**, *9*, 591−598.
(24) Figge, L.; Hacker, N. P.; Lefferts, S. WO 9847945, October 29, 1998.
(25) Figge, L.; Hacker, N. P.; Lefferts, S. WO 9847944, October 29, 1998.
(26) Ou, D. L.; Chevalier, P. M.; Mackinnon, I. A.; Eguchi, K.; Boisvert, R.; Su, K. *J. Sol-Gel Sci. Technol.* **2003**, *26*, 407−412.
(27) Bujalski, D. R.; Eguchi, K.; Gordon, G. V.; Hu, S.; Ou, D. L.; Su, K. *J. Mater. Chem.* Submitted.
(28) Terry, K. W.; Ganzel; P. K.; Tilley, T. D. *Chem. Mater.* **1992**, *4*, 1290−1295.
(29) Terry, K. W.; Tilley, T. D. *Chem. Mater.* **1991**, *3*, 1001−1003.
(30) Terry, K. W.; Lugmair, C. G.; Gantzel, P. K.; Tilley, T. D. *Chem. Mater.* **1996**, *8*, 274−280.
(31) Su, K.; Tilley, T. D. *Chem. Mater.* **1997**, *9*, 588−595.
(32) Terry, K. W.; Lugmair, C. G.; Tilley, T. D. *J. Am. Chem. Soc.* **1997**, *119*, 9745−9756.
(33) Fujdala, K. L.; Tilley, T. D. *Chem. Mater.* **2002**, *14*, 1376−1384.
(34) Lugmair, C. G.; Fujdala, K. L.; Tilley, T. D. *Chem. Mater.* **2002**, *14*, 888−898.
(35) Brutchey, R. L.; Goldberger, J. E.; Koffas, T. S.; Tilley, T. D. *Chem Mater.* **2003**, *15*, 1040−1046.
(36) Van de Grampel, J. C.; Puyenbroek, R.; Rousseeuw, B. A. C.; van der Drift, E. W. J. M. Silicon-containing resist materials Based on Chemical Amplification. In *ACS Symp. Ser. (Inorganic and Organometallic Polymers II)* **1994**, *572*, 81−91.
(37) Su, K.; Tilley, T. D. *J. Am. Chem. Soc.* **1996**, *118*, 3459−3468.
(38) Abe, Y.; Gunji, T.; Kimata, Y.; Kuramata, M.; Kasgoz, A.; Misono, T. *J. Non-Crystalline Solids* **1990**, *121*, 21−25
(39) Brunauer, S.; Emmett, P. H.; Teller, E. *J. Am. Chem. Soc.* **1938**, *60*, 309−319.
(40) Barrett, E. P.; Joyner, L. G.; Halenda, P. P. *J. Am. Chem. Soc.* **1951**, *73*, 373.

Table 1. Summary of $(HSiO_{3/2})_x[(^tBuO)SiO_{3/2}]_z$ Resin Synthesis

reference	theoretical composition	composition by ^{29}Si and ^1H NMR	$HSi(OEt)_3$ (g)	$(AcO)_2SiO^tBu)_2$ (g)	water (g)	yield (g) appearance
IA	$(HSiO_{3/2})_{0.20}[(^tBuO)SiO_{3/2}]_{0.80}$	$(HSiO_{3/2})_{0.21}[(^tBuO)SiO_{3/2}]_{0.79}$	5.67	40.2	6.1	23.7, gum
IIA	$(HSiO_{3/2})_{0.40}[(^tBuO)SiO_{3/2}]_{0.60}$	$(HSiO_{3/2})_{0.43}[(^tBuO)SiO_{3/2}]_{0.57}$	11.23	30.0	6.65	18.7, gum
IIIA	$(HSiO_{3/2})_{0.60}[(^tBuO)SiO_{3/2}]_{0.40}$	$(HSiO_{3/2})_{0.62}[(^tBuO)SiO_{3/2}]_{0.38}$	16.85	20.0	7.2	15.4, solid
IVA	$(HSiO_{3/2})_{0.70}[(^tBuO)SiO_{3/2}]_{0.30}$		20.0	26.2	10.0	*a*
VA	$(HSiO_{3/2})_{0.75}[(^tBuO)SiO_{3/2}]_{0.25}$		22.4	10.0	7.8	gel

[a] Not isolated, stored in methylisobutyl ketone (MIBK).

Table 2. Summary of $(HSiO_{3/2})_x(RSiO_{3/2})_y[(^tBuO)SiO_{3/2}]_z$ Silsesquioxane Synthesis

reference	theoretical composition	composition by ^{29}Si NMR	$HSi(OEt)_3$ (g)	$(AcO)_2Si(O^tBu)_2$ (g)	$(MeO)_3Si-(CH_2)_{17}CH_3$ (g)	H_2O (g)	toluene (g), body step	yield (g) appearance
IB	$(HSiO_{3/2})_{0.45}(RSiO_{3/2})_{0.15}[(^tBuO)SiO_{3/2}]_{0.40}$	$(HSiO_{3/2})_{0.46}(RSiO_{3/2})_{0.13}[(^tBuO)SiO_{3/2}]_{0.41}$	25.3	40.0	19.3	14.4	250	43.6, oil
IIB	$(HSiO_{3/2})_{0.40}(RSiO_{3/2})_{0.20}[(^tBuO)SiO_{3/2}]_{0.40}$	$(HSiO_{3/2})_{0.41}(RSiO_{3/2})_{0.19}[(^tBuO)SiO_{3/2}]_{0.40}$	22.5	40.0	25.7	14.4	250	46.7 oil
IIIB	$(HSiO_{3/2})_{0.65}(RSiO_{3/2})_{0.20}[(^tBuO)SiO_{3/2}]_{0.15}$		36.5	20.0	25.6	16.4	250	44.4, oil
IVB	$(HSiO_{3/2})_{0.55}(RSiO_{3/2})_{0.20}[(^tBuO)SiO_{3/2}]_{0.25}$	$(HSiO_{3/2})_{0.54}(RSiO_{3/2})_{0.22}[(^tBuO)SiO_{3/2}]_{0.24}$	12.4	10.0	10.3	6.7	110	19.6, wax
VB	$(HSiO_{3/2})_{0.50}(RSiO_{3/2})_{0.10}[(^tBuO)SiO_{3/2}]_{0.40}$	$(HSiO_{3/2})_{0.49}(RSiO_{3/2})_{0.09}[(^tBuO)SiO_{3/2}]_{0.42}$	29.0	40.8	10.3	14.0	120	37.0 wax

of approximately 15%. The reduced modulus, $E_R = E/(1-\nu^2)$, where E and ν are the Young's modulus and Poisson's ratio, respectively, was determined from the slope of the unloading curve. The reported values are the average of three indents measured at different areas of the film.

Dynamic Mechanical Thermal Analysis. DMTA was conducted using a Rheometric Scientific RDAII equipped with rectangular torsion fixtures. A solution of the test sample (35−40 wt %) was absorbed into a 45 mm × 6.3 mm × 0.68 mm binder-free glass fiber filter GF/D (Aldrich Z25, 829-6) substrate, and the solvent was evaporated under vacuum. A dynamic frequency of 1 rad s^{-1} was used with a strain less than 0.3%. A thermal ramp of 3 °C min^{-1} in nitrogen—up to 500 °C—was employed.

Atomic Force Microscopy. A Dimension 5000 atomic force microscope was used in tapping mode to collect height and amplitude images at 5-μm scan sizes. The X and Y calibration was 10 μm ± 0.5 μm. The Z sensitivity was 180 nm ± 1 nm.

Synthesis of $(HSiO_{3/2})_x[(^tBuO)SiO_{3/2}]_z$ Silsesquioxanes from $HSi(OEt)_3$ and $(AcO)_2Si(O^tBu)_2$. A summary of the synthesis of $(HSiO_{3/2})_x[(^tBuO)SiO_{3/2}]_z$ is provided in Table 1. In a typical procedure, mixtures of $(AcO)_2Si(O^tBu)_2$ and $HSi(OEt)_3$ were dissolved into 72 g of THF in a flask under argon. Deionized water was then added to the solution and the mixture was stirred at room temperature for 1 h. Toluene (75 g) was added to the solution and the solvent was removed using a rotary evaporator at 30−38 °C and less than 10 mmHg pressure, which yielded a viscous oil that was immediately redissolved into 150 g of toluene. The solvent was evaporated again using a rotary evaporator to remove residual HOAc via HOAc/toluene azeotrope. The residual material was then dissolved in 110 g of toluene and azeotropically dried and condensed between 100 and 110 °C for 1 h. The solution was filtered and the solvent was evaporated to give the final product.

The $(HSiO_{3/2})_x[(^tBuO)SiO_{3/2}]_z$ silsesquioxane exhibited two groups of resonances in the −70 to −90 ppm and −90 to −115 ppm ranges from the T^H and Q silicon nuclei, respectively. The relative intensity of the peaks depends on the resin composition and the data for IIIA are given as a representative example.

^{29}Si NMR ($CDCl_3$, δ): −75.9 ppm ($H(HO)SiO_{2/2}$), −85.6 ppm ($HSiO_{3/2}$), −94.5 ppm (($^tBuO)(HO)SiO_{2/2}$), −96.4 ppm, −97.6 ppm (($^tBuO)_2SiO_{2/2}$), −101.5 ppm ($(HO)SiO_{3/2}$), −105.5 ppm (($^tBuO)SiO_{3/2}$), −112 ppm ($SiO_{4/2}$).

^1H NMR ($CDCl_3$, δ): 1.31 ppm (O^tBu), 4.38 ppm (SiH), 3.6 to 4.0 ppm (SiOH).

^{13}C NMR ($CDCl_3$, δ): 31.5 ppm ($C(CH_3)_3$, 73.8 ppm ($C(CH_3)_3$).

FTIR Spectra (film on KBr, cm^{-1}): 3412 (vs), 2777 (vs), 2248 (s), 1392 (m), 1367 (m), 1474, (m), 1392 (m), 1367 (m), 1240 (m), 1065 (s), 862 (s) 701 (s).

Synthesis of $(HSiO_{3/2})_x(RSiO_{3/2})_y[(^tBuO)SiO_{3/2}]_z$ Silsesquioxanes from $HSi(OEt)_3$, $RSi(OMe)_3$ [$R = (CH_2)_{17}CH_3$], and $(AcO)_2Si(O^tBu)_2$. A summary of the synthesis of $(HSiO_{3/2})_x(RSiO_{3/2})_y[(^tBuO)SiO_{3/2}]_z$ is shown in Table 2. In a typical procedure, $(AcO)_2Si(OtBu)_2$, $RSi(OMe)_3$, and $HSi(OEt)_3$ were dissolved into 75 g of THF in a flask under argon. Deionized water was then added to the solution and the mixture was stirred at room temperature for 1 h. Toluene (75 g) was added to the solution and solvent was removed using a rotary evaporator (38 °C, <10 mmHg pressure) leading to a viscous oil, which was immediately redissolved into 150 g of toluene. The solvent was evaporated again using a rotary evaporator to remove residual HOAc via HOAc/toluene azeotrope. The residue was then dissolved into 250 g of toluene and azeotropically dried and condensed between 100 and 110 °C for 1 h. The solution was filtered and the solvent was evaporated to give the final product.

The $(HSiO_{3/2})_x(RSiO_{3/2})_y[(^tBuO)SiO_{3/2}]_z$ silsesquioxane exhibited three groups of resonances in the −50 to −70 ppm, −70 to −90 ppm, and −90 to −115 ppm ranges from the T^R, T^H, and Q silicon nuclei, respectively. The relative intensities of the peaks depended on composition, and the data for IIB are given as a representative example.

^{29}Si NMR ($CDCl_3$, δ): −56.0 ppm ($R(HO)SiO_{2/2}$), −64.3 ppm ($RSiO_{3/2}$), −75.9 ppm ($H(HO)SiO_{2/2}$), −84.7 ppm ($HSiO_{3/2}$), −93.4 ppm (($^tBuO)(HO)SiO_{2/2}$), −95.3 and −96.4 ppm (($^tBuO)_2SiO_{2/2}$), −101.0 ppm ($(HO)SiO_{3/2}$), −103.3 ppm (($^tBuO)SiO_{3/2}$), −109 ppm ($SiO_{4/2}$).

^1H NMR ($CDCl_3$, δ): 0.65 ppm, 0.87 ppm, 1.25 ppm (O^tBu), 1.32 ppm, 4.32 ppm (SiH), 3.5 to 4.0 ppm (SiOH).

^{13}C NMR ($CDCl_3$, δ): 14.1 ppm, 22.7 ppm, 29.3 ppm, 29.7 ppm ($C(CH_3)_3$), 31.3 ppm, 31.9 ppm, 73.8 ppm ($C(CH_3)_3$).

FTIR Spectra (film on KBr, cm^{-1}): 3398 (s), 2976 (vs), 2918 (vs), 2845 (vs), 2251 (s), 1894 (w), 1745 (m), 1714 (m), 1464 (s), 1387 (m), 1366 (s), 1240, (m), 1054 (vs), 862 (s), 712 (s).

Resin Pyrolysis. An aliquot of the resin sample was weighed into an alumina crucible and transferred into a tube furnace. The

Table 3. Summary of Pyrolysis Results (450 °C for 2 h Under Argon) for $(HSiO_{3/2})_x[(^tBuO)SiO_{3/2}]_z$ and $(HSiO_{3/2})_x(RSiO_{3/2})_y[(^tBuO)SiO_{3/2}]_z$

sample reference	composition	resin (g)	char (g)	yield wt %	calc. wt.%[b]	TGA 450 °C
IA	$(HSiO_{3/2})_{0.21}[(^tBuO)SiO_{3/2}]_{0.79}$	2.10	0.96	45.8	53.3	46.0
IIA	$(HSiO_{3/2})_{0.43}[(^tBuO)SiO_{3/2}]_{0.57}$	2.07	1.06	51.4	60.6	53.9
IIIA	$(HSiO_{3/2})_{0.62}[(^tBuO)SiO_{3/2}]_{0.38}$	2.01	1.22	60.6	69.3	62.2
IVA[a]	$(HSiO_{3/2})_{0.70}[(^tBuO)SiO_{3/2}]_{0.30}$	1.83	1.18	64.5	73.4	
VA[a]	$(HSiO_{3/2})_{0.75}[(^tBuO)SiO_{3/2}]_{0.25}$	2.20	1.63	74.2	77.1	77.6
IB	$(HSiO_{3/2})_{0.46}(RSiO_{3/2})_{0.13}[(^tBuO)SiO_{3/2}]_{0.41}$	2.15	1.11	51.9	46.6	56.4
IIB	$(HSiO_{3/2})_{0.41}(RSiO_{3/2})_{0.19}[(^tBuO)SiO_{3/2}]_{0.40}$	2.01	1.07	53.0	42.0	53.2
IIIB[a]	$(HSiO_{3/2})_{0.65}(RSiO_{3/2})_{0.20}[(^tBuO)SiO_{3/2}]_{0.15}$	2.20	1.19	53.9	47.2	57.9
IVB	$(HSiO_{3/2})_{0.54}(RSiO_{3/2})_{0.22}[(^tBuO)SiO_{3/2}]_{0.24}$	2.05	1.27	61.8	44.9	58.2
VB	$(HSiO_{3/2})_{0.49}(RSiO_{3/2})_{0.09}[(^tBuO)SiO_{3/2}]_{0.42}$	2.02	1.23	60.8	51.1	62.6

[a] Composition based on the ratio of starting materials. [b] Assuming an average one *tert*-butoxy group per Q silicon and loss of all R and O^{t}Bu groups.

furnace was then evacuated to less than 20 Torr and backfilled with argon. Under a purge of argon, the sample was heated to a designated temperature at 10 °C/min and held at temperature for 2 h before cooling to room temperature. The pyrolysis conditions and yields are summarized in Table 3.

Material Derived from IIIA. ^{29}Si NMR (MAS, δ) −83.7 ppm ($HSiO_{3/2}$), −100 ppm (shoulder, $(HO)SiO_{3/2}$), −109.3 ppm ($SiO_{4/2}$). Composition obtained from MAS ^{29}Si NMR: $T^H_{0.37}Q_{0.63}$. Anal. Found: C, 1.76%; H, 2.09%. DRIFT Spectra (KBr powder, cm^{-1}): 3466 (m), 2959 (m), 2258 (s), 1652 (w), 1050 (vs), 877 (vs).

Material Derived from IA. ^{29}Si NMR (MAS, δ): −83.4 ppm ($HSiO_{3/2}$), −100 ppm (shoulder, $(HO)SiO_{3/2}$), −109.6 ppm ($SiO_{4/2}$). Composition obtained from MAS ^{29}Si NMR: $T^H_{0.08}Q_{0.92}$. Anal. Found: C, 2.80%; H, 1.82%.

Material Derived from VB. ^{29}Si NMR (MAS, δ): −64.1 ppm ($RSiO_{3/2}$), −84.8 ppm ($HSiO_{3/2}$), −109.3 ppm ($SiO_{4/2}$). ^{13}C NMR (CP/MASS, δ): 58.9 ppm, 30.0 ppm, 23.8 ppm, 15.9 ppm, 11.9 ppm, 3.9 ppm, −6.6 ppm. Anal. Found: C, 7.13%; H, 2.29%. DRIFT Spectra (KBr powder, cm^{-1}): 3742 (m), 2963 (vs), 2929 (vs), 2263 (vs), 1636 (w), 1277 (m), 1050 (vs), 877 (vs), 816(s). For IB Anal. Found: C, 12.19%; H, 2.81%. For IIB Anal. Found: C, 14.71%; H, 3.65%. For IIIB Anal. Found: C, 11.88%; H, 3.45%. For IVB Anal. Found: C, 19.75%; H, 4.66%.

Coatings and Thin Film Formation. An aliquot of each silsesquioxane was dissolved in MIBK to form a 20−25 wt % clear solution. The solution was sequentially filtered through 1.0- and 0.2-μm syringe membrane filters to remove any large particles. The solution was applied to the silicon wafer and spun-coated at 2000 rpm for 20 s on a silicon wafer using either a Karl Suss RC8 or a Headway spin coater. The thickness of the as-spun films, ranging from 200 to 2000 nm, was controlled by a combination of solution concentration and spin speed. The resin films were loaded into a QTF furnace and quickly heated to 450 °C under nitrogen. The coated wafers were heated at this temperature for 2 h, and subsequently cooled to room temperature. All the coated wafers were stored in a nitrogen atmosphere before the property measurements.

Results and Discussion

Resin Synthesis and Characterization. $(HSiO_{3/2})_x[(^tBuO)SiO_{3/2}]_z$ silsesquioxanes were synthesized according to eq 1. Samples of $HSi(OEt)_3$ and $(AcO)_2Si(O^tBu)_2$ were first hydrolyzed in tetrahydrofuran (THF), followed by distillation of acetic acid byproduct and further condensation in reflux toluene. The removal of the acetic acid from the reaction mixture before applying heat was crucial in obtaining a soluble material. Silsesquioxanes with at least 40 mol % Q ($SiO_{4/2}$) were isolated as brittle solids. Materials with 70 mol % SiH were unstable in solid form, but remained soluble when stored in MIBK solution at −4 °C. When the $HSiO_{3/2}$ content was above 70 mol %, the material gelled during preparation.

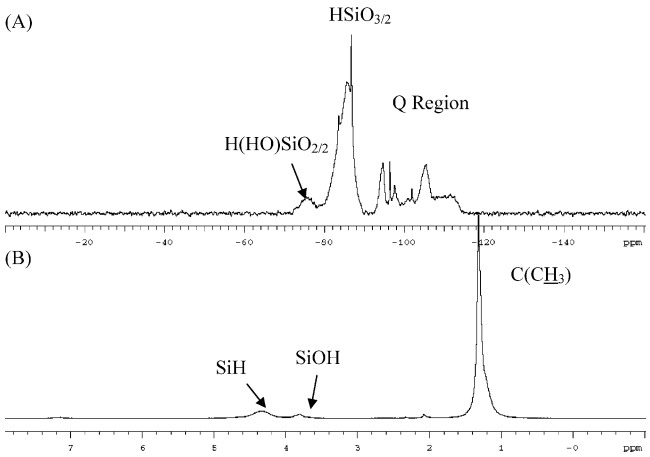

Figure 1. ^{29}Si (A) and ^{1}H (B) NMR spectra of $(HSiO_{3/2})_{0.62}[(^tBuO)SiO_{3/2}]_{0.38}$ (IIIA).

$$x\mathrm{HSi(OEt)_3} + z(^t\mathrm{BuO})_2\mathrm{Si(OAc)_2} + \mathrm{H_2O\ (exc.)} \rightarrow (\mathrm{HSiO_{3/2}})_x[(^t\mathrm{BuO})\mathrm{SiO_{3/2}}]_z \quad (1)$$

A typical ^{29}Si nuclear magnetic resonance (NMR) spectrum of the $(HSiO_{3/2})_x[(^tBuO)SiO_{3/2}]_z$ silsesquioxanes is shown in Figure 1A. This silsesquioxane exhibited two groups of resonances in the −70 to −90 ppm and −90 to −115 ppm range from the $HSiO_{3/2}$ and $SiO_{4/2}$ silicon nuclei, respectively. The group of resonances in the −90 to −115 ppm region were attributed to $SiO_{4/2}$ (−112 ppm), $(HO)SiO_{3/2}$ (−101.5 ppm), $(^tBuO)SiO_{3/2}$ (−105.5 ppm), $(^tBuO)(HO)SiO_{2/2}$ (−94.5 ppm), and $(^tBuO)_2SiO_{2/2}$ (−96 to −99 ppm). The ^{1}H NMR spectrum in Figure 1B displayed resonances from $OC(CH_3)_3$ (1.27 ppm), Si*H* (4.38 ppm), and SiO*H* or $SiOCH_2CH_3$ (3.6−4.0 ppm) protons.[41] The presence of the Si−O^{t}Bu group was also detected using ^{13}C NMR (31.5 ppm for CH_3 and 73.8 ppm for CMe_3). On the basis of the ratio of $RSiO_{3/2}$/$SiO_{4/2}$ and O^{t}Bu/SiH mole ratios determined from the ^{29}Si NMR and ^{1}H NMR spectra, there was slightly more than one O^{t}Bu on average $SiO_{4/2}$ silicon, indicating existence of $(^tBuO)_2SiO_{2/2}$ structure. The presence of SiH (2248 cm^{-1}) and SiOH (broad, 3420 cm^{-1}) was also evident in the infrared (IR) spectrum.[41]

(41) Dijkstra, T. W.; Duchateau, R.; Van Santen, R. A.; Meetsma, A.; Yap, G. P. A. *J. Am. Chem. Soc.* **2002**, *124*, 9856−9864.

The $(HSiO_{3/2})_x(RSiO_{3/2})_y[(^tBuO)SiO_{3/2}]_z$ silsesquioxanes were synthesized by cohydrolysis and condensation of $(AcO)_2Si(O^tBu)_2$, $HSi(OEt)_3$, and $CH_3(CH_2)_{17}Si(OMe)_3$, as shown in eq 2.

$$xHSi(OEt)_3 + yCH_3(CH_2)_{17}Si(OMe)_3 + z(^tBuO)_2Si(OAc)_2 + H_2O\ (exc.) \rightarrow (HSiO_{3/2})_x(RSiO_{3/2})_y[(^tBuO)SiO_{3/2}]_z \quad (2)$$

As with $(HSiO_{3/2})_x[(^tBuO)SiO_{3/2}]_z$, it was essential to remove the acetic acid to obtain soluble $(HSiO_{3/2})_x(RSiO_{3/2})_y[(^tBuO)SiO_{3/2}]_z$ materials. The final products were isolated as low T_g (<30 °C) materials that were stable in solid form over months at 0 °C and the stability can be further improved by storing in methyl isobutyl ketone (MIBK) solution. The ^{29}Si NMR spectra of $(HSiO_{3/2})_x(RSiO_{3/2})_y[(^tBuO)SiO_{3/2}]_z$ (Figure 2) exhibited three groups of resonances at −50 to −70 ppm, −70 to −90 ppm, and −90 to −115 ppm arising from the $RSiO_{3/2}$, $HSiO_{3/2}$, and the $SiO_{4/2}$ silicon nuclei, respectively. A significant amount of residual $R(HO)SiO_{2/2}$ units (near 50 mol % of total $RSiO_{3/2}$) was observed in the NMR spectra of all silsesquioxanes. Similar to $(HSiO_{3/2})_x[(^tBuO)SiO_{3/2}]_z$, the Q (−90 to −115 ppm) region contains a mixture of resonances arising from the $SiO_{4/2}$, $(HO)SiO_{3/2}$, $(^tBuO)_2SiO_{2/2}$, $(^tBuO)(HO)SiO_{2/2}$, and $(^tBuO)SiO_{3/2}$ structural units. The ^{13}C NMR spectra of $(HSiO_{3/2})_x(RSiO_{3/2})_y[(^tBuO)SiO_{3/2}]_z$ exhibit resonances corresponding to the carbon nuclei for the *tert*-butyl group at 31.5 ppm (CH_3) and 73.8 ppm (CMe_3), as well as the resonances arising from the octadecyl moiety. The $(HSiO_{3/2})_x(RSiO_{3/2})_y[(^tBuO)SiO_{3/2}]_z$ compositions (Table 1) determined by ^{29}Si NMR analysis were consistent with stoichoimetric incorporation of monomers into the silsesquioxanes structure.

Molecular Weight Analysis. The molecular weight analysis was obtained by size exclusion chromatography (SEC) using refractive index, viscosity, and light-scattering detectors. The viscosity detector measures the intrinsic viscosity $[\eta]$ whereas the light-scattering detector provides information about the absolute size of the molecule, which is described by the weight-average molecular weight M_w and the radius of gyration R_g. From these data, the dependence of $[\eta]$ on M_w can be used to infer the relative extent of branching and any conformational differences existing between materials.

The molecular weight, radius of gyration, and conformational properties of the $(HSiO_{3/2})_x[(^tBuO)SiO_{3/2}]_z$ silsesquioxanes were a function of the T/Q ratio. Figure 3 shows that at similar reaction conditions, both the molecular weight and polydispersity increased with increasing $HSiO_{3/2}$ content, which was consistent with the observation that silsesquioxanes with high SiH content were less stable. These results may suggest that alkoxy groups limited molecular growth due to steric hindrance and, therefore, enhanced the stability of the silsesquioxanes. The molecular weight distribution for $(HSiO_{3/2})_x(RSiO_{3/2})_y[(^tBuO)SiO_{3/2}]_z$ silsesquioxanes showed less obvious trend on material composition. Most of the silsesquioxanes exhibited a broad molecular weight distribution with M_w/M_n in the range of 3.5−4.5.

Table 4 summarizes the molecular weight results of $(HSiO_{3/2})_x[(^tBuO)SiO_{3/2}]_z$ and $(HSiO_{3/2})_x(RSiO_{3/2})_y[(^tBuO)SiO_{3/2}]_z$. For $(HSiO_{3/2})_x[(^tBuO)SiO_{3/2}]_z$, R_g increased from 1.6 to 4.7 nm as the T/Q ratio increased from 0.27 to 1.63. The Mark−Houwink (M−H) exponent[42,43] of $(HSiO_{3/2})_x[(^tBuO)SiO_{3/2}]_z$ decreased from 0.24 to 0.14 as the $(^tBuO)SiO_{3/2}$ content increased from 38 to 79 mol % or as M_w decreased by over an order of magnitude. Empirically, the M−H exponent can provide information with respect to molecular shape, where the limits are $a = 0$ for hard spheres and 2 for rigid rods. Hence, the $(HSiO_{3/2})_x[(^tBuO)SiO_{3/2}]_z$ silsesquioxanes with a lower $HSiO_{3/2}/(^tBuO)SiO_{3/2}$ ratio, or smaller molecular size (M or R_g), appeared to have a more spherical conformation, possibly due to the highly branched structure, as well as presence of bulky *tert* butoxy group. The molecular size and shape of the $(HSiO_{3/2})_x(RSiO_{3/2})_y[(^tBuO)SiO_{3/2}]_z$ silsesquioxanes were between 0.22 and 0.30, also consistent with a compact structure.

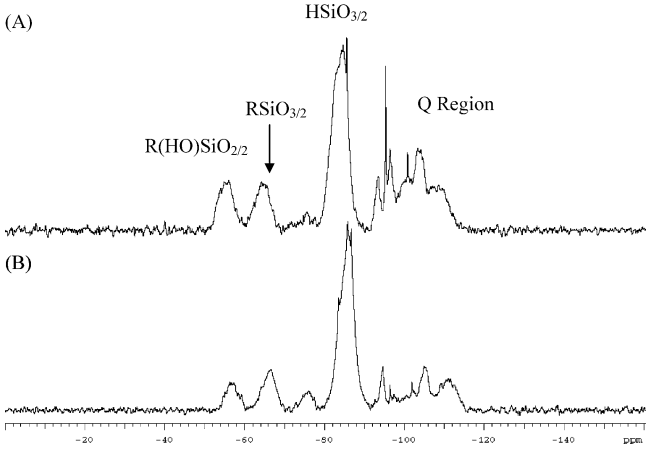

Figure 2. ^{29}Si NMR spectrum of (A) $(HSiO_{3/2})_{0.41}(RSiO_{3/2})_{0.19}[(^tBuO)SiO_{3/2}]_{0.40}$ (IIB) and (B) $(HSiO_{3/2})_{0.54}(RSiO_{3/2})_{0.22}[(^tBuO)SiO_{3/2}]_{0.24}$ (IVB).

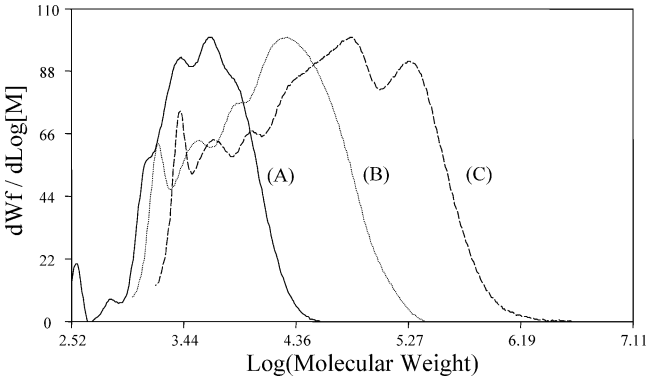

Figure 3. Molecular weight distribution for (A) $(HSiO_{3/2})_{0.21}[(^tBuO)SiO_{3/2}]_{0.79}$ (IA); (B) $(HSiO_{3/2})_{0.43}[(^tBuO)SiO_{3/2}]_{0.57}$ (IIA); and (C) $(HSiO_{3/2})_{0.62}[(^tBuO)SiO_{3/2}]_{0.38}$ (IIIA).

Silsesquioxane Cure and High-Temperature Decomposition Chemistry. The cure and the decomposition processes were studied using dynamic mechanical thermal analysis (DMTA) by monitoring the temperature dependence of the dynamic mechanical shear properties of the silsesquioxane embedded in an inert glass substrate. By comparing the DMTA and thermogravimetric analysis (TGA) results, physical transitions, such as the glass transition and cure temperatures, and chemical decomposition events can be

(42) Mark, H. In *Der feste Körper*; Sänger, R., Ed.; Hirzel: Leipzig, 1938.
(43) Houwink, R. *J. Prakt. Chem.* **1940**, *157*, 15−18.

Table 4. Size Exclusion Chromatographic Analysis of $(HSiO_{3/2})_x[(^tBuO)SiO_{3/2}]_z$ and $(HSiO_{3/2})_x(RSiO_{3/2})_y[(^tBuO)SiO_{3/2}]_z$ Silsesquioxanes

sample	composition from ^{29}Si NMR	M_n (g mol^{-1})	M_w (g mol^{-1})	M_w/M_n	$[\eta]_w$ (dL g^{-1})	Rg_w (nm)	M−H (a)
IA	$(HSiO_{3/2})_{0.21}[(^tBuO)SiO_{3/2}]_{0.79}$	3040	6300	2.1	0.023	1.6	0.14
IIA	$(HSiO_{3/2})_{0.43}[(^tBuO)SiO_{3/2}]_{0.57}$	6750	25 800	3.8	0.024	2.5	0.19
IIIA	$(HSiO_{3/2})_{0.62}[(^tBuO)SiO_{3/2}]_{0.38}$	15 000	136 000	9.0	0.039	4.7	0.24
IB	$(HSiO_{3/2})_{0.46}(RSiO_{3/2})_{0.13}[(^tBuO)SiO_{3/2}]_{0.41}$	9360	72 100	7.7	0.048	4.2	0.28
IIB	$(HSiO_{3/2})_{0.41}(RSiO_{3/2})_{0.19}[(^tBuO)SiO_{3/2}]_{0.40}$	5660	80 200	14.2	0.053	4.4	0.22
IVB	$(HSiO_{3/2})_{0.54}(RSiO_{3/2})_{0.22}[(^tBuO)SiO_{3/2}]_{0.24}$	8270	35 900	4.3	0.046	3.5	0.30

easily identified. Figure 4 shows that the elastic storage modulus, G', of $(HSiO_{3/2})_{0.41}(RSiO_{3/2})_{0.19}[(^tBuO)SiO_{3/2}]_{0.40}$ (IIB) decreased upon heating and exhibited a minimum near 60 °C. The decrease was attributed to the glass−liquid transition of the silsesquioxane. A further increase in temperature resulted in an increase in the modulus indicating the onset of cure. The further increase in modulus starting at 350 °C, which corresponded to the start of a weight-loss event from the TGA data, was consistent with structural reorganization due to elimination of the *tert* butoxy groups.

TGA coupled with evolved gas analysis (EGA) was used to help elucidate the high-temperature decomposition chemistry. As shown in Figure 5, the decomposition of $(HSiO_{3/2})_{0.7}[(^tBuO)SiO_{3/2}]_{0.3}$ (IVA), which started around 150 °C and ended by 450 °C, occurred as a two-step weight loss, with the second process starting at 360 °C. The volatiles coming off of the resins at 190 °C and 407 °C were collected in cold traps. The total ion chromatograms (TIC) for the volatile materials collected at 190 and 407 °C traps for the

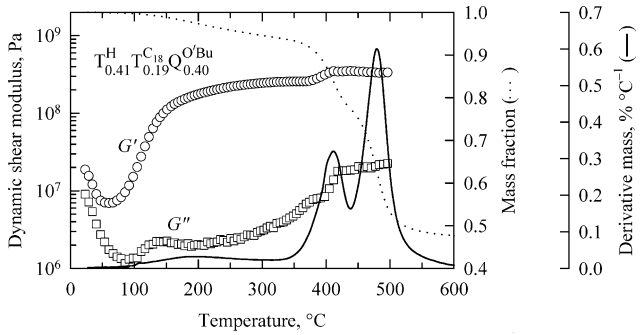

Figure 4. Cure and decomposition profiles of $(HSiO_{3/2})_{0.41}(RSiO_{3/2})_{0.19}[(^tBuO)SiO_{3/2}]_{0.40}$ (IIB) by dynamic mechanical thermal (frequency of 1 rad s^{-1}, 3 °C min^{-1} in N_2) and thermogravimetric (10 °C min^{-1} in He) analyses, respectively.

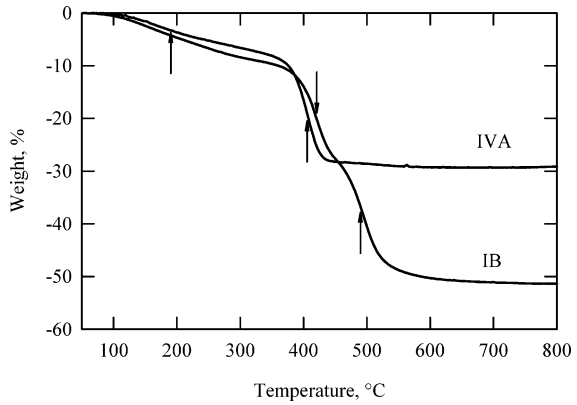

Figure 5. TGA profile for $(HSiO_{3/2})_{0.70}[(^tBuO)SiO_{3/2}]_{0.30}$ (IVA) and $(HSiO_{3/2})_{0.46}(RSiO_{3/2})_{0.13}[(^tBuO)SiO_{3/2}]_{0.41}$ (IB). The arrows (190 and 407 °C for IVA; 420 and 490 °C for IB) indicate the temperatures at which evolved gases from the decomposition processes were collected and analyzed.

$(HSiO_{3/2})_{0.7}[(^tBuO)SiO_{3/2}]_{0.3}$ silsesquioxane are shown in Figure 6. The 190 °C trap contained water (1.3 min), *t*-BuOH (1.7 min), and several partially hydrolyzed monomers at higher retention times. The compounds collected from the 407 °C trap were composed mainly of isobutene (1.3 min), along with trace amounts of EtOH and *t*-BuOH.

A decomposition mechanism for the *tert*-butoxy containing silsesquioxanes can be proposed based on the distribution of the decomposition products at various temperatures. The decomposition processes, outlined in eqs 3−5, involve the initial elimination of *t*-BuOH and water by silanol/silanol or SiOH/SiO^{t}Bu condensation during the curing process at fairly low temperatures. Upon the depletion of the silanol groups, the ^{t}BuO group is eliminated by formation of isobutene and silanol, as shown in eq 5. Such a process has been reported to be catalyzed by an acid.[28,29] The presence of high concentration of silanol in the cured materials was verified by MAS ^{29}Si NMR and IR analyses.

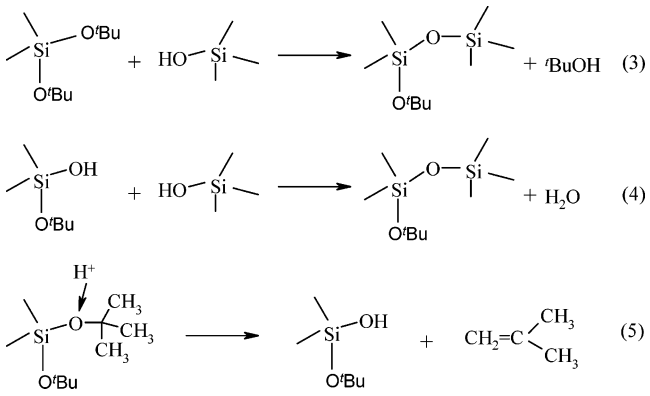

The TGA-EGA of the $(HSiO_{3/2})_{0.46}(RSiO_{3/2})_{0.13}[(^tBuO)SiO_{3/2}]_{0.41}$ (IB, R = octadecyl) silsesquioxane confirmed the stepwise decomposition of the two porogen groups. The TGA profile in Figure 5 shows three weight loss events that range from 150 to 400 °C, 400 to 450 °C, and 450 to 500 °C. Figure 7 shows the TICs for the evolved gases collected at 420 (top) and 490 °C (bottom). The evolved gases between 400 and 450 °C consisted of EtOH (1.46 min), ^{t}BuOH (1.6 min), and isobutene (1.32 min). At temperatures above 450 °C, hydrocarbons with various chain lengths resulting from the decomposition of the octadecyl group were observed. The decomposition chemistry for the alkyl group was consistent with a random free radical cleavage reaction of carbon−carbon bond.

Bulk Pyrolysis, Material Composition, and Porosity. The bulk pyrolysis of $(HSiO_{3/2})_x[(^tBuO)SiO_{3/2}]_z$ and $(HSiO_{3/2})_x(RSiO_{3/2})_y[(^tBuO)SiO_{3/2}]_z$ silsesquioxanes at 450 °C for 2 h under argon produced off-white or transparent materials with yields as summarized in Table 3. The yields for the

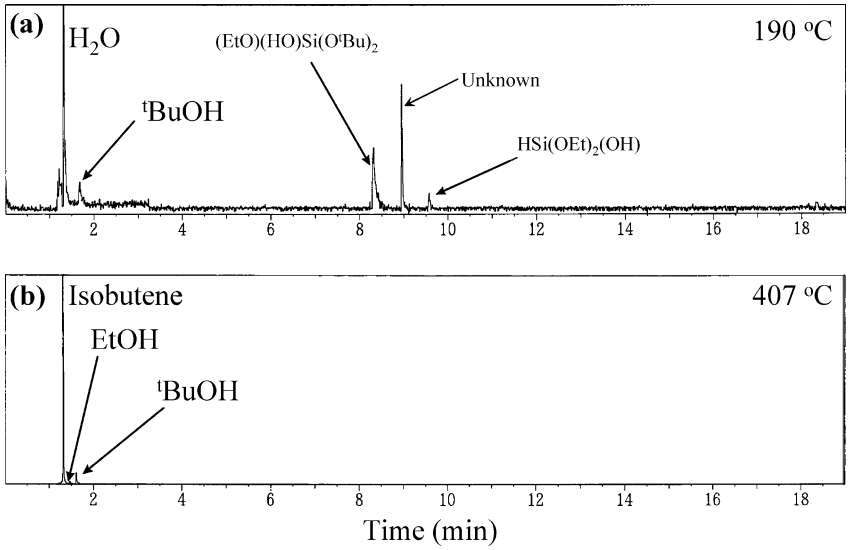

Figure 6. Total ion chromatograms of gases, evolved during the decomposition of $(HSiO_{3/2})_{0.70}[(^tBuO)SiO_{3/2}]_{0.30}$ (IVA), that were collected at (a) 190 °C and (b) 407 °C.

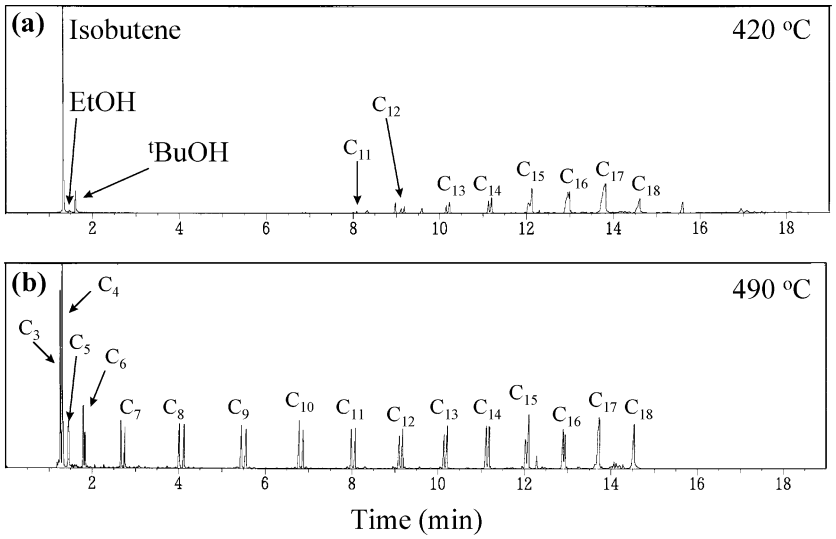

Figure 7. Total ion chromatograms of gases, evolved during the decomposition of $(HSiO_{3/2})_{0.46}(RSiO_{3/2})_{0.13}$ $[(^tBuO)SiO_{3/2}]_{0.41}$ (IB), that were collected at (a) 420 °C and (b) 490 °C.

$(HSiO_{3/2})_x[(^tBuO)SiO_{3/2}]_z$ materials were lower than the theoretical weight retention assuming one *tert* butoxy group on each Q silicon and complete loss of *tert* butoxy group. This result can be explained by evaporation of oligomers or presence of $(O^tBu)_2SiO_{2/2}$, $SiO_{4/2}$ groups, and silanol-containing structures that are not accounted for in the calculation. The elemental analysis of pyrolyzed $(HSiO_{3/2})_{0.62}[(^tBuO)SiO_{3/2}]_{0.38}$ and $(HSiO_{3/2})_{0.70}[(^tBuO)SiO_{3/2}]_{0.30}$ resins showed 1.76 and 2.80 wt % carbon, respectively. The solid-state ^{29}Si MAS NMR spectra of chars derived from $(HSiO_{3/2})_{0.62}[(^tBuO)SiO_{3/2}]_{0.38}$ (IIIA) and $(HSiO_{3/2})_{0.21}[(^tBuO)SiO_{3/2}]_{0.79}$ (IA) revealed a resonance arising from $HSiO_{3/2}$ (−83.7 ppm) and $SiO_{4/2}$ (−109.3 ppm), as well as $(HO)SiO_{3/2}$ (shoulder near −100 ppm, Q_3). A significant reduction in the SiH/Q ratio suggested a SiH/SiOH condensation reaction during the thermolysis.

The yields at 450 °C for $(HSiO_{3/2})_x(RSiO_{3/2})_y[(^tBuO)SiO_{3/2}]_z$ silsesquioxanes were close to the observed weight retention at 450 °C by TGA (Table 3), but approximately 10 to 14% higher than the theoretical yield assuming complete loss of the organics (R and O^{t}Bu). The retention of carbon (7−20%) was also supported by elemental analysis. The MAS ^{29}Si NMR spectrum for material derived from $(HSiO_{3/2})_{0.50}(RSiO_{3/2})_{0.10}[(^tBuO)SiO_{3/2}]_{0.40}$ (VB) silsesquioxane, Figure 8A, exhibited resonances that can be assigned to $RSiO_{3/2}$ (−64.2 ppm), $HSiO_{3/2}$ (−84.8 ppm), and $SiO_{4/2}$ (−109.3 ppm). Similar to $(HSiO_{3/2})_x[(^tBuO)SiO_{3/2}]_z$, a reduction in the $HSiO_{3/2}/SiO_{4/2}$ ratio was also observed. The pyrolyzed material contained a higher mole percentage of the $R^*SiO_{3/2}$ (R = alkyl) structure ($(HSiO_{3/2})_{16}(R^*SiO_{3/2})_{0.16}[(^tBuO)SiO_{3/2}]_{0.68}$) than in the precursor ($(HSiO_{3/2})_{0.50}(RSiO_{3/2})_{0.10}[(^tBuO)SiO_{3/2}]_{0.40}$). The ^{13}C CP/MAS NMR spectrum, Figure 8B shows resonances that can be attributed to T^{Me} (−5 ppm) and alkyl groups with various chain lengths. Residual silanols were also observed in the ^{29}Si MAS NMR spectra for selected bulk samples.

The Brunauer−Emmett−Teller[39] (BET) surface area and total pore volume for heat-treated $(HSiO_{3/2})_x[(^tBuO)SiO_{3/2}]_z$ resins are summarized in Table 5. The porosity and BET surface areas both rapidly increased when the ^{t}BuOSiO$_{3/2}$

Table 5. Density and Porosity of $(HSiO_{3/2})_x[(^tBuO)SiO_{3/2}]_z$ and $(HSiO_{3/2})_x(RSiO_{3/2})_y[(^tBuO)SiO_{3/2}]_z$ Silsesquioxanes

sample	composition	skeletal density (g/cm^3)	calc. density for inorg. (g/cm^3)	BET surface area (m^2/g)	total pore volume (cc/g)	porosity (V/V%)[b]	theor. porosity (V/V%)
IA	$(HSiO_{3/2})_{0.21}[(^tBuO)SiO_{3/2}]_{0.79}$	1.970	1.98	550	0.313	38.1	66.6
IIA	$(HSiO_{3/2})_{0.43}[(^tBuO)SiO_{3/2}]_{0.57}$	1.982	1.85	559	0.317	38.6	58.1
IIIA	$(HSiO_{3/2})_{0.62}[(^tBuO)SiO_{3/2}]_{0.38}$	1.873	1.75	454	0.260	32.7	47.2
IVA[a]	$(HSiO_{3/2})_{0.70}[(^tBuO)SiO_{3/2}]_{0.30}$	1.787	1.71	392	0.224	28.6	41.6
VA[a]	$(HSiO_{3/2})_{0.75}[(^tBuO)SiO_{3/2}]_{0.25}$	1.719	1.69	413	0.241	29.3	31.6
IB	$(HSiO_{3/2})_{0.46}(RSiO_{3/2})_{0.13}[(^tBuO)SiO_{3/2}]_{0.41}$	1.669	1.84	1213	0.701	53.9	73.5
IIB	$(HSiO_{3/2})_{0.41}(RSiO_{3/2})_{0.19}[(^tBuO)SiO_{3/2}]_{0.40}$	1.638	1.87	1123	0.678	52.6	77.0
IIIB[a]	$(HSiO_{3/2})_{0.65}(RSiO_{3/2})_{0.20}[(^tBuO)SiO_{3/2}]_{0.15}$	1.337	1.74	1007	0.623	45.4	73.1
IVB	$(HSiO_{3/2})_{0.54}(RSiO_{3/2})_{0.22}[(^tBuO)SiO_{3/2}]_{0.24}$	1.346	1.80	534	0.349	32.0	74.9
VB	$(HSiO_{3/2})_{0.49}(RSiO_{3/2})_{0.09}[(^tBuO)SiO_{3/2}]_{0.42}$	1.751	1.82	882	0.515	47.4	69.9

[a] Composition based on the ratio of starting materials. [b] Calculated from skeletal density and measure pore volume.

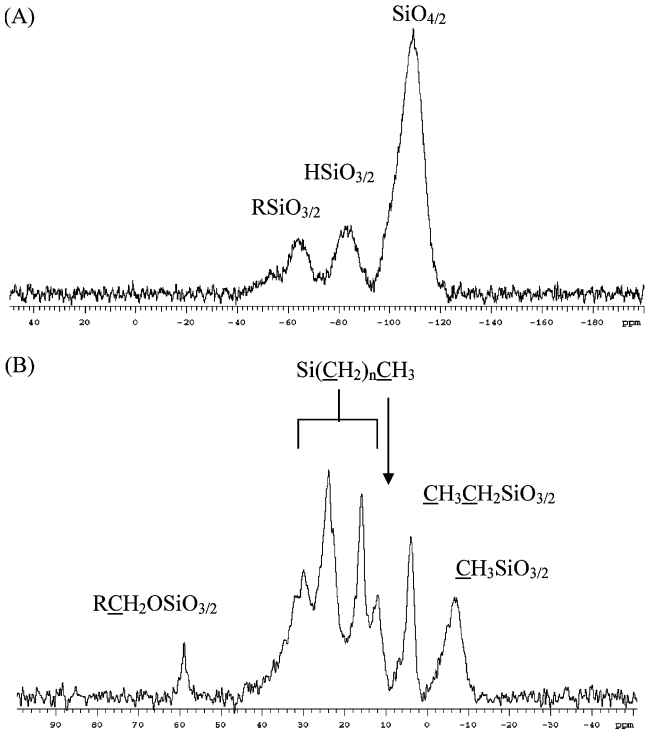

Figure 8. Solid-state NMR spectra of the pyrolysis product from $(HSiO_{3/2})_{0.49}(RSiO_{3/2})_{0.09}$ $[(^tBuO)SiO_{3/2}]_{0.42}$ (VB) by (A) ^{29}Si MAS and (B) ^{13}C CP/MAS.

content in the silsesquioxane increased from 0 to 25 mol % and then they leveled off at approximately 0.241 cm^3/g and 413 m^2/g, respectively. The total pore volume and BET surface area of the pyrolyzed $(HSiO_{3/2})_x(RSiO_{3/2})_y[(^tBuO)SiO_{3/2}]_z$ silsesquioxanes (2 h at 450 °C) ranged from 0.44 to 0.70 cm^3/g and from 669 to 1213 m^2/g, respectively. By taking into account the matrix density or skeletal density, the porosity of these materials can be calculated from the measured total pore volume. The materials derived from $(HSiO_{3/2})_x[(^tBuO)SiO_{3/2}]_z$ were found to have porosity between 28.6 and 38.6%, while those for $(HSiO_{3/2})_x(RSiO_{3/2})_y[(^tBuO)SiO_{3/2}]_z$ ranged from 32 to 54%. The results indicated an increase in porosity of around 10%, when a second porogen, the octadecyl group, was incorporated into the silsesquioxane structure.

To understand the effect of material composition and thermal treatment on porosity, the volume fraction of the organic component in the precursor was calculated from the silsesquioxane composition determined from NMR analysis. It was assumed the density for the "organic" component was the same as octadecane (0.87 g/cm^3). The density of the "inorganic" component was calculated from the density of "SiO_2" (2.11 g/cm^3)[44] and "$HSiO_{3/2}$" (1.57 g/cm^3)[45] by assuming both $RSiO_{3/2}$ and $(^tBuO)SiO_{3/2}$ were converted to SiO_2, while $HSiO_{3/2}$ remained unchanged after the thermal treatment.[46] As shown in Table 5, the calculated density for the inorganic component was similar to or slightly lower than the skeletal density of $(HSiO_{3/2})_x[(^tBuO)SiO_{3/2}]_z$, as measured by helium pycnometry. The lower value was attributed to conversion of $HSiO_{3/2}$ to $SiO_{4/2}$, which was supported by MAS ^{29}Si NMR. Both the calculated and skeletal densities of the materials derived from $(HSiO_{3/2})_x[(^tBuO)SiO_{3/2}]_z$ expectedly increased with increasing $(^tBuO)SiO_{3/2}$ content. The skeletal densities for $(HSiO_{3/2})_x(RSiO_{3/2})_y[(^tBuO)SiO_{3/2}]_z$ showed a less obvious trend and were generally lower than the calculated densities especially for silsesquioxanes with higher R contents. This result supports the retention of organics in the pyrolyzed materials.

Assuming all the volume occupied by the organic groups was converted to pores, the theoretical porosity was calculated from the silsesquioxane composition and the known densities of the organic and inorganic components. In Table 5 the results are compared with the porosity derived from the measured pore volume and skeletal density. The observed porosity for $(HSiO_{3/2})_x[(^tBuO)SiO_{3/2}]_z$ was generally lower than the calculated value, with larger derivation being observed for resins with higher $(^tBuO)SiO_{3/2}$ contents. Clearly, pore collapse occurred during thermal treatment. The observed porosities of materials derived from $(HSiO_{3/2})_x(RSiO_{3/2})_y[(^tBuO)SiO_{3/2}]_z$ showed less correlation with the calculated values. The decrease in porosity was attributed to densification due to the Si−C and Si−O bond redistribution reactions that occur above 400 °C.[47,48] The results can be compared with porous materials derived from sol−gel route,[49,50] in which the final porosity depends on not only

(44) Skeletal density of "SiO_2" derived from $[(^tBuO)SiO_{3/2})]_n$ by heating at 450 °C.

(45) The density of $(HSiO_{3/2})_n$ measured by helium pyconometry was used in the calculation.

(46) The density of inorganic component $d = Wtd_1d_2/(Wt_1d_2 + Wt_2d_1)$, where Wt is the formula weight of resin after thermal conversion of $RSiO_{3/2}$ and $(^tBuO)SiO_{3/2}$ to SiO_2, while Wt_1 and Wt_2 are the weight of $HSiO_{3/2}$ and $SiO_{4/2}$ structural units, respectively. d_1 (1.57 g/cm^3) and d_2 (2.11 g/cm^3) are the density of "$HSiO_{3/2}$" and "SiO_2", respectively.

(47) Burns, G. T.; Taylor, R. B.; Xu, Y.; Zangvil, A.; Zank, G. A. *Chem. Mater.* **1992**, *4*, 1313−1323.

(48) Bujalski, D. R.; Grigoras, S.; Lee, W−l; Wieber, G. M.; Zank, G. A. *J. Mater. Chem.* **1998**, *8*, 1427−1433.

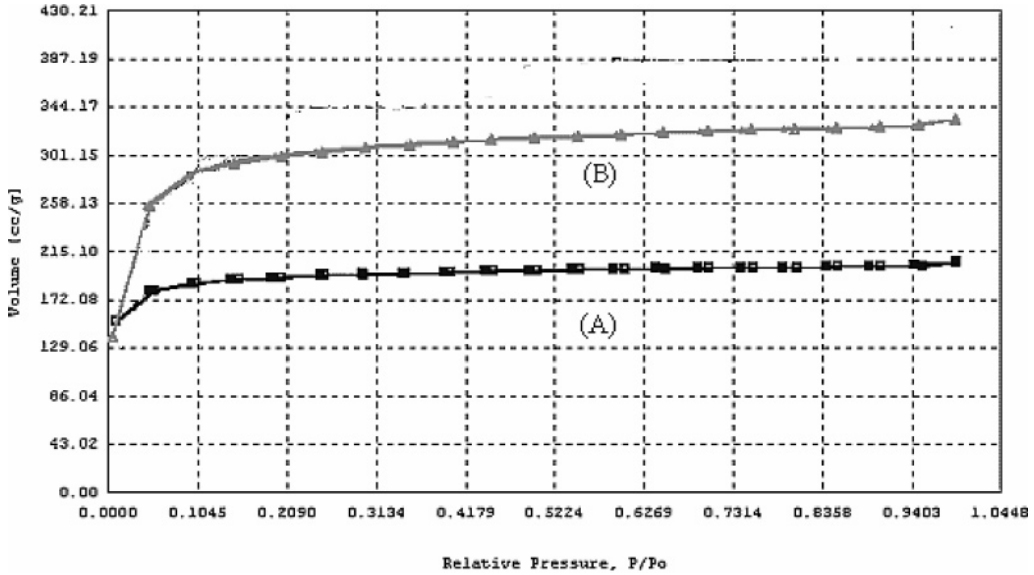

Figure 9. Nitrogen adsorption/desorption isotherms of selected cured resins: (A) $(HSiO_{3/2})_{0.43}[(^tBuO)SiO_{3/2}]_{0.57}$ (IIA) and (B) $(HSiO_{3/2})_{0.49}(RSiO_{3/2})_{0.09}[(^tBuO)SiO_{3/2}]_{0.42}$ (VB)

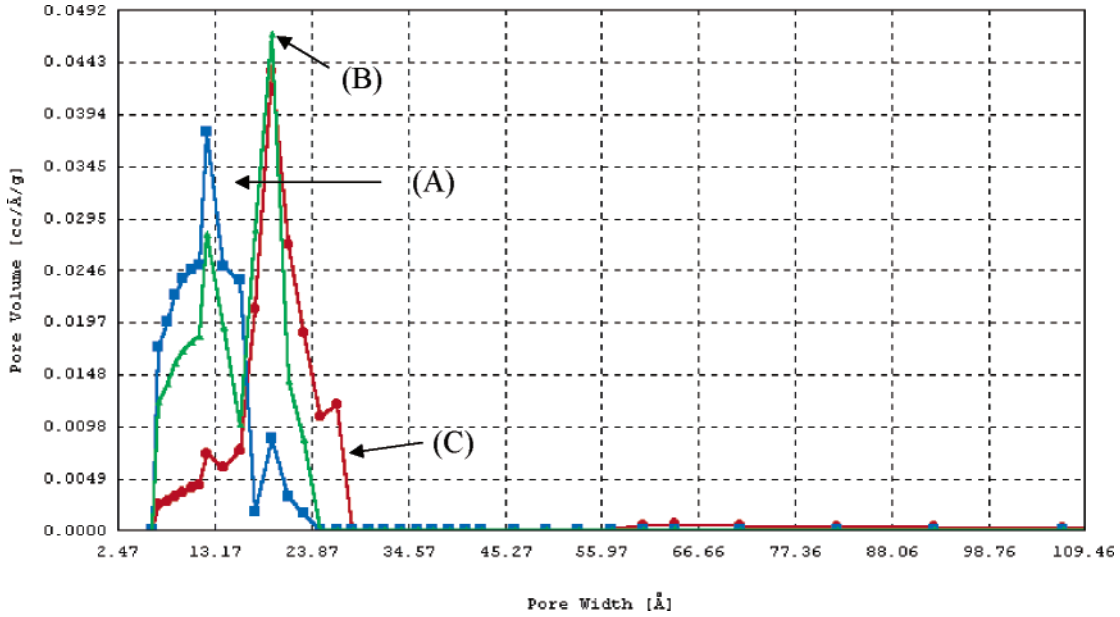

Figure 10. DFT pore size distributions of selected cured resins: (A) $(HSiO_{3/2})_{0.43}[(^tBuO)SiO_{3/2}]_{0.57}$ (IIA), (B) $(HSiO_{3/2})_{0.49}(RSiO_{3/2})_{0.09}$ $[(^tBuO)SiO_{3/2}]_{0.42}$ (VB), and (C) $(HSiO_{3/2})_{0.30}(RSiO_{3/2})_{0.22}$ $[(^tBuO)SiO_{3/2}]_{0.48}$.

the organic content, but also the structural rigidity that supports the porosity.

Figure 9 shows the nitrogen adsorption/desorption isotherms for selected $(HSiO_{3/2})_x[(^tBuO)SiO_{3/2}]_z$ and $(HSiO_{3/2})_x(RSiO_{3/2})_y[(^tBuO)SiO_{3/2}]_z$ silsesquioxanes. On the high relative-pressure side, the isotherms of both $(HSiO_{3/2})_{0.43}[(^tBuO)SiO_{3/2}]_{0.57}$ (IIA) and $(HSiO_{3/2})_{0.10}(RSiO_{3/2})_{0.50}[(^tBuO)SiO_{3/2}]_{0.40}$ (VB) silsesquioxanes were reversible and with no hysteresis. The isotherms appeared to be typical Type I isotherms, indicating that the pore sizes did not exceed a few adsorbate molecular diameters which, once filled with the nitrogen, leave little or no external surface for additional adsorption. The complete overlap of the adsorption and desorption isotherms suggested an open pore structure.

The pore size distributions of the $(HSiO_{3/2})_x[(^tBuO)SiO_{3/2}]_z$ and $(HSiO_{3/2})_x(RSiO_{3/2})_y[(^tBuO)SiO_{3/2}]_z$ silsesquioxanes were calculated using the Barrett−Joyner−Halenda[40] (BJH) and density functional theory[51] (DFT) methods. The result from the DFT is shown in Figure 10. The distribution curves obtained using the BJH method indicated that all the pores were less than 5 nm. The $(HSiO_{3/2})_x[(^tBuO)SiO_{3/2}]_z$ silsesquioxanes contained pore sizes around 1.1 nm. For the materials derived from $(HSiO_{3/2})_x(RSiO_{3/2})_y[(^tBuO)SiO_{3/2}]_z$, the DFT method revealed a bimodal pore size distribution (1.1 and 2.3 nm). As a comparison, a $(HSiO_{3/2})_{0.30}(RSiO_{3/2})_{0.22}[SiO_{4/2}]_{0.48}$ silsesquioxane that is without the O^{t}Bu group was

(49) *Sol−Gel Science: The Physics and Chemistry of Sol−Gel Processing*; Brinker, C. J.; Scherer, G. W.; Academic Press: San Diego, CA, 1990; Chapter 9, pp 515−609.
(50) Shea, K. J.; Loy, D. A. *Chem. Mater.* **2001**, *13*, 3306−3319.
(51) Evans, R.; Marconi, U. M. B.; Tarazona, P. *J. Chem. Soc., Faraday Trans. 2* **1986**, *82*, 1763.

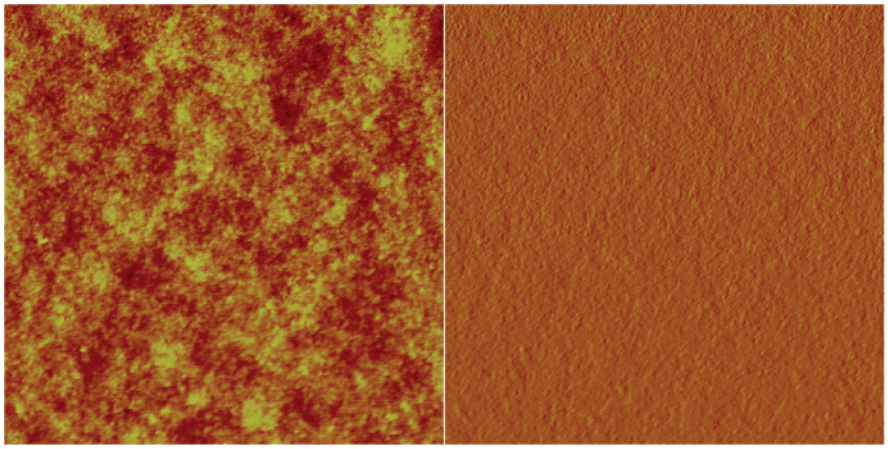

Figure 11. Tapping mode (5 × 5 μm^2) AFM height (left) and amplitude (right) images of film prepared from IVA.

Table 6. Thin Film Properties of $(HSiO_{3/2})_x[(^tBuO)SiO_{3/2}]_z$ and $(HSiO_{3/2})_x(RSiO_{3/2})_y[(^tBuO)SiO_{3/2}]_z$ Silsesquioxanes

reference	*k*	modulus (GPa)	hardness (GPa)	thickness (nm)	refractive index
IA	24.3	18.6	0.88	418	1.348
IA	14.9	16.1	0.77	412	1.355
IIIA	4.89	12.1	0.96	988	1.247
IVA	6.34	10.8	1.06	659	1.290
IB	2.30	3.4	0.53	940	1.186
IIB	1.97	2.1	0.36	1180	1.173
IIIB	1.70	1.8	0.31	1502	1.178
IVB	2.55	4.7	0.80	492	1.288
VB	2.25	4.4	0.36	1453	-

prepared by an independent route.[52] After thermal treatment, the material exhibited only single peak centered at 2.3 nm resulting from the thermal decomposition of dodecyl group. The bimodal pore size distribution for $(HSiO_{3/2})_x(RSiO_{3/2})_y[(^tBuO)SiO_{3/2}]_z$ appeared to be related to the presence of two porogens in the precursor materials.

Thin Film Properties. The silsesquioxanes were spin-coated onto the wafers and heat-treated at 450 °C for 2 h under an argon atmosphere. The surface morphology was studied using atomic force microscope (AFM) and the result for IVA is shown in Figure 11. A height image can be directly correlated to surface topography, while amplitude images typically enhance the textural and morphological features of the surface. The average roughness (Ra) for the film derived from IVA is 0.28 nm (RMS 0.35; Z = 3.69 nm), which suggests a very smooth surface.

The dielectric constants for the films derived from $(HSiO_{3/2})_x[(^tBuO)SiO_{3/2}]_z$ silsesquioxanes, shown in Table 6, were high (5−25 at 10^6 Hz), but decreased with increasing SiH content. The higher dielectric constants were consistent with the presence of residual silanol in the films. This was confirmed by IR analysis, which revealed a broad SiOH peak at 3500 cm^{-1}. The residual silanol concentration increased with increasing ^{t}BuOSi content, which was consistent with the isobutene elimination decomposition mechanism of SiO^tBu established by TGA-EGA. The low efficiency of the SiH/SiOH condensation reaction mechanism in eliminating the silanol groups is attributed to the high rigidity of the network structure (>10 GPa). Potentially, it might be viable to cap the silanol with a chemical reagent to lower the dielectric constant, as in the case of porous glass. The dielectric constant of films derived from $(HSiO_{3/2})_x(RSiO_{3/2})_y[(^tBuO)SiO_{3/2}]_z$ ranged from 1.7 to 2.6, where the lowest value corresponded to IIIB.

The modulus of films derived from $(HSiO_{3/2})_x[(^tBuO)SiO_{3/2}]_z$ silsesquioxanes increase with increasing Q content in the starting materials despite a higher level of porosity expected from O^{t}Bu-rich materials. The modulus for the thin films derived from $(HSiO_{3/2})_x(RSiO_{3/2})_y[(^tBuO)SiO_{3/2}]_z$ resins ranged from 1.2 to 4.7 GPa and were lower than those for $(HSiO_{3/2})_x[(^tBuO)SiO_{3/2}]_z$. The trend with Q content was less obvious presumably due to the presence of residual organics from incomplete decomposition and higher level of porosity.

Conclusions

This paper described the synthesis, characterization, and properties of two new silsesquioxanes that contained a bulky alkoxy group, $(HSiO_{3/2})_x[(^tBuO)SiO_{3/2}]_z$ and $(HSiO_{3/2})_x(RSiO_{3/2})_y[(^tBuO)SiO_{3/2}]_z$ (R = octadecyl). The good stability of these materials was attributed to the bulky *tert* butoxy group, which could retard the hydrolysis of Si−O^{t}Bu bond. Upon heating, this alkoxy group decomposed to produce porous silsesquioxane resins that were modified with "silica". The high modulus of films derived from $(HSiO_{3/2})_x[(^tBuO)SiO_{3/2}]_z$ silsesquioxanes indicated the effectiveness to improve the mechanical properties of porous materials through in situ generation of Q structure. By incorporation of a second organic porogen, materials with over 50% porosity were achieved. The films derived from $(HSiO_{3/2})_x(RSiO_{3/2})_y[(^tBuO)SiO_{3/2}]_z$ had low *k* and somewhat improved modulus and can be used as interlayer dielectric coatings.

Acknowledgment. We thank M. J. Spaulding, C. R. Yeakle, J. L. Dingman, T. L. Sanders, Jr., D. K. Bailey, D. F. Fenner, and R. K. King for assistance in carrying out this work.

CM048993D

(52) Chung, K.; King, R. K.; Zhang, S.; Zhong, B. U.S. patent 6,359,096.